Heliyon 9 (2023) e17672

Contents lists available at ScienceDirect

Heliyon

journal homepage: www.cell.com/heliyon

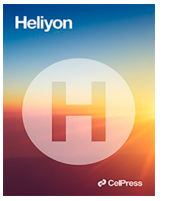

Freeze-thaw cycle and abrasion resistance of alkali-activated FA and POFA-based mortars: Role of high volume GBFS incorporation

Ghasan Fahim Huseien [a,*], Masoumeh Khamehchi [b], Ziyad Kubba [c], Omrane Benjeddou [d], Mohammad Javad Mahmoodi [b,**]

[a] Institute of Architecture and Construction, South Ural State University, Lenin Prospect 76, 454080 Chelya-binsk, Russia
[b] Faculty of Civil, Water & Environment Engineering, Shahid Beheshti University, Tehran, Iran
[c] Department of Civil Engineering, College of Engineering, Al-Muthanna University, 66001 Samawa, Iraq
[d] Prince Sattam Bin Abdulaziz University, College of Engineering, Department of Civil Engineering, Alkharj, 16273, Saudi Arabia

ARTICLE INFO

Keywords:
Eco-friendly binder
Alkali-activated materials
High volume slag
Freezing-thawing
Abrasion resistance

ABSTRACT

Alkali-activated binders made from various waste products can appreciably reduce the emission of CO_2 and enhance the waste recycling efficiency, thus making them viable substitutes to ordinary Portland cement (OPC)-based binders. Waste materials including fly ash (FA), palm oil fuel ash (POFA), and granulated blast furnace slag (GBFS) reveal favorable effects when applied to alkali-activated mortars (AAMs) that are mainly related to the high contents of silica, alumina, and calcium. Therefore, fifteen AAM mixes enclosing FA, POFA with high volume of GBFS were designed. The obtained GBFS/FA/POFA-based AAMs were subjected wet/dry and freeze/thaw cycles. The impact of various GBFS contents on the microstructures, freeze-thaw cycle, abrasion resistance, mechanical and durability features of the proposed AAMs were evaluated. The results showed that presence of Ca can significantly affect the AAMs durability features and long-term performance. The abrasion resistance of the AAMs was decreased with the decrease of CaO contents. Furthermore, the abrasion depth of 70% AAMs (0.8 mm) was lower in comparison to the mix made by replacing 50 wt% of FA with GBFS (1.4 mm). Generally, increase in the GBFS contents from 50 to 70% could largely impact the AAMs properties under aggressive environmental exposure. The expansion and physical impacts during the freezing-thawing cycles was argued to destroy the bonds in *C*–S–H and paste-aggregates, causing the formation of large cracks. It is asserted that the AAM mixes made from FA, POFA and high volume of GBFS may offer definitive mechanical, durable, and environmental benefits with their enhanced performance under aggressive environments.

1. Introduction

Traditional cement production produces significant amounts of carbon dioxide and consumes a great deal of energy [1,2]. Reduction in the emission of CO_2 is a major issue for the cement industries worldwide due to the production of vast amount of cement [3,4]. Many studies showed that geopolymers (GPs) can serve as viable alternatives to OPC, reducing the greenhouse gases emission.

* Corresponding author.
** Corresponding author.
E-mail addresses: eng.gassan@yahoo.com (G.F. Huseien), mj_mahmoudi@sbu.ac.ir (M.J. Mahmoodi).

https://doi.org/10.1016/j.heliyon.2023.e17672
Received 12 February 2023; Received in revised form 25 June 2023; Accepted 25 June 2023
Available online 27 June 2023

Thus GPs-based concrete can lower the greenhouse gases emission about 80% lower than OPC and 26–45% lesser compared to OPC concretes [5–8]. GPs are the generic term that can be applied for the alkaline solid alumina-silicates reaction for the production of hardened binders made by combining the hydrous alkali-alumina-silicates and/or alkali-alkali earth-alumina-silicates [9]. More accurately, GPs serve as a promising green building material. The polymerization reactions that take place between alumina-silicate-rich material and alkali activation result in the production of geopolymer concretes (GPCs). They are obtained from many sources such as FA, POFA and GBFS. It has great mechanical qualities and durability, which significantly lowers production-related energy uses and emission of greenhouse gases [10]. FA is a typical precursor cementing component generated as a spin-off in the power plant [11]. The dissolved silica, aluminum, and other ions are polycondensed and polymerized when an alkaline media activates them, creating a substance with mechanical qualities similar to Portland cement [12]. Higher fineness and the usage of activators are typically used to increase FA's responsiveness [13].

Geopolymerization requires the alumina-silicate oxides to be dissolved in alkali poly-silicate, producing Si–O–Al bonds and semi-crystalline alumina-silicate structure in 3D with chemical formula Mn [–(Si–O_2)z–Al–O]n.wH_2O (where M is the alkali metal, z that can be 1, 2, 3, or more is the extent of polycondensation or polymerization). Geopolymers come in three key forms, namely, poly (sialate), poly (sialate-siloxo), and poly (sialate-disiloxo) with the corresponding Si to A1 ratio of 1, 2, and 3. It was recommended to use the SiO_2 to M_2O and SiO_2 to Al_2O_3 molar ratio in the range of 4.0–6.6 and 5.5 to 6.5 for alkali poly (sialate-disiloxo) with the Si to Al ratio of 3, respectively [14,15]. Other researchers have identified similar ranges for the molar ratios of M_2O to SiO_2 ranged from 0.2 to 0.48, SiO_2 to Al_2O_3 ranged from 3.3 to 4.5, and H_2O to M_2O ranged from 10 to 25. This displays the need for an optimal molar proportion of SiO_2 to Al_2O_3, and an effective alkali medium such as Na, K- hydroxide or a Na_2SiO_3 solution to activate the alkali. Typically, NaOH and Na2SiO3 are used to form an alkali solution wherein OH^- facilitates the feedstock's dissolution of Si^{4+} and Al^{3+}. Meanwhile, Na^+ facilitates the crystallization of the GPs. Both high and low quantities of Na+ impact the mixture's compressive strength and thus the ratio of Na_2SiO_3 to NaOH is critical in this process. Lower Na^+ and OH levels prevent full dissolution and polymerization, whilst higher levels of Na^+ content leave excess Na+ in the specimen, which weakens the geopolymers structure. Morsy et al. [16] showed that an increase in the NaOH to Na_2SiO_3 ratio from 0.5 to 1.00 can increase the strengths of FA-based GPs. Natural resources like metakaolin and kaolinite together with other waste materials from diverse industries like FA, waste glass, slag, and soil waste can be used as the sources of aluminate-silicate precursors for geopolymers production [17]. Subsequently, these can then be applied to various alkaline dosages during activation procedures and under different curing conditions.

Vast quantities of POFA, or waste materials from palm oil by-products, are generated in a number of agricultural sectors throughout Thailand, Malaysia, and Indonesia. Furthermore, it is anticipated that increased palm oil tree planting in these areas will cause a steady increase in POFA production. The creation of POFA requires the burning of oil palm clinkers, shells, and empty fruit bunches. According to a survey conducted in 2007, Thailand and Malaysia produce several million tonnes of POFA annually and this figure is steadily rising [1]. It is interesting to note that due to its zero commercial value, POFA is generally thrown as landfill into lagoon, which poses a severe environmental risk. Nonetheless, recent research has demonstrated that high silica content POFA may be advantageous for sustainable growth of the construction sectors. This advancement has promoted research into the topic, as well as extensive use of the inexpensive and widely accessible resource material (POFA). Moreover, POFA is a pozzolanic agent, indicating its effective uses as a binder in GPs or part of replacement for OPC in conventional concretes to increase their strength and durability performance.

High-curing temperatures are necessary in facilitating quick and effective geopolymerization whilst also retaining the required compressive strengths (CS). This is critical in producing GPs using just FA. For FA-based GPC the values of early compressive strength (CS) can reach to 5 MPa at 60 °C after three days of curing. This can be a drawback in alkali-activated FA products. However, it seems that the addition of GBFS to FA can help to develop a GPC that has an acceptable CS upon ambient temperature curing. The waste by-product GBFS is outsourced from the quenched molten iron slag produced in a blast furnace under water or steam. Then, the amorphous and granular by-product is ground after drying to get a fine powder. The slag properties can vary considerably depending on the raw materials' chemical composition during the manufacturing of iron. GBFS disply both cementitious and pozzolanic characteristics because of high CaO and SiO_2 contents. Many studies have been conducted that the inclusion GBFS in cement and GPs significantly improve the strength performance [18,19]. The structures of *N*-A-*S*-H gels are created when lower quantities of calcium FA are used. Thus, CaO found in GBFS facilitates the formation of *C*-A-*S*-H and *C*–S–H gels [20,21]. In turn, this heightens the alkalinity of the mixture and generates a water deficiency. By encouraging quicker and greater alumina-silicate dissolution, improve alkaline condition can improve the geopolymerizations and poly-condensation processes at room temperature. Moreover, the CS is can be enhanced by adding GBFS. Nonetheless, the study revealed that excessive GBFS material accelerates the setup procedure. Geopolymer binders (GPBs) were used to create the appropriate strength and a workable setting time in this research. Meanwhile, preliminary research indicates that the amount of GBFS in the mixture should be maintained at 30%. For above 30% of GBFS, the setting time decreases but the strength increases, making the production of GP feasible at ambient temperature.

Many factors including aggregate content, size, component ratios, porosity, admixtures, and binder types can affect the engineering attributes of GPs in various ways. There are two categories of these factors like aggregate gradation and GP pastes (GPPs). Nonetheless, studies examining how they interact and impact the mechanical qualities of previous concrete are scarce. The intricate impact of binder types and CaO content on geopolymerization requires more research. Additionally, the majority of earlier studies employed high temperatures to cure the GPs. Nevertheless, it is important to cure GPCs at room temperature before their practical applications [22]. As far as the researcher is aware, very few studies have examined the impacts that high volume GBFS, FA and POFA have on characteristics of designed AAMs, especially with POFA. Thus, this study focused on developing a mixed design strategy for creating high-volume slag GPs using FA and POFA and establishing ambient temperature curing conditions. Based on reaction byproducts, AAMs surface morphology observations, and mechanical characteristics of manufactured samples, the optimal GBFS concentrations were determined.

2. Methodology

2.1. Materials characterization

In this work, NaOH and Na_2SiO_3 were used as alkali activators, whereas waste raw materials like FA, POFA, and GBFS were utilized to design the proposed AAMs. Additionally, the fine aggregates used here included river sands. The binder was made without cement using pure GBFS (obtained from Malaysia) as a constituent as it is. This slag, which has an off-white colour, stands out from other auxiliary cementitious materials because it possesses both pozzolanic and cementitious characteristics. When water was added, the reaction occurred, forming GBFS. XRF spectra of GBFS showed that it was mostly consisted of calcium (51.8%), silicate (30.8%), and alumina (10.9%). AAMs were made using FA and POFA (alumina-silicate components with a low calcium content) which was collected from a Power Station and palm oil mills (Malaysia). These materials were grey-coloured and met the ASTM C618 standard [23]. Compared to GBFS, FA and POFA included 5.2% and 10.2% calcium, 57.2% and 64.2% silicate, and 28.8% and 4.3% aluminum, respectively (Table 1). It also complied with these specifications. The median size of particles in FA, POFA and GBFS (Fig. 1) measured using a particle size analyzer was 10 μm, 8.2 μm and 12.8 μm, respectively. BET surface are of FA and GBFS was calculated to assess the physical properties and CSs. POFA had larger specific surface area (of 23.1 m^2/g) compared to FA (18.1 m^2/g) and GBFS (13.6 m^2/g). Fig. 2 displays the appearance of FA (grey), POFA (dark grey) and GBFS (off-white).

XRD profiles (Fig. 2) of FA, POFA and GBFS showed pronounced diffraction peaks at 2θ values between 16 and 30°, indicating the existence of alumina and silica crystallites. However, the presence of additional sharp peaks was due to the existence of crystalline quartz and mullite phases. In fact, their genuine disorder was verified by the XRD analysis of GBFS that lacked any intense peaks. The presence of calcium and silica was vital for the development of GBFS. The large amounts of silica and calcium in glassy form that reacted in the GBFS were beneficial for the synthesis of AAMs. However, the low levels of Al_2O_3 (10.49 wt%) in GBFS had to be overcome, and thus FA was introduced. SEM pictures of FA, POFA, and GBFS showed that FA was composed of regular spherical grains, whereas POFA and GBFS were composed of uneven and angular grains, thus in agreement with the previous reports [24].

The suggested mortars were prepared using fine aggregates made of river sand with a saturated surface. Based on ASTM C117 [25] standard guidelines, it was rinsed with water to decrease the presence of silts and pollutants. After removing the moisture, the AAMs were dried in an oven at 60 °C (24 h) before being scored to match ASTM C33 [26] requirements. Prepared aggregates had fineness modulus and specific gravity of 2.9 and 2.6, respectively. Pellets of analytical grade NH (98% purity) were added to water and dissolved in order to create a solution containing a 4-M concentration. Moreover, NS mix consists of SiO_2 (29.5 wt%), Na_2O (14.70 wt%), and H_2O (55.80 wt%) was used. After the M NH solution was produced, it was left to cool for 24 h and then it was combined with NS mixture to make an ultimate alkaline solution with SiO_2 to Na_2O ratio of 1.2. For all alkali solutions, NS to NH ratio was kept constant at 0.75.

2.2. Mix design preparation

For all the proposed mortar mixtures, the binder to fine aggregate ratio (B:A), alkaline activator solution to binder ratio (S:B) were correspondingly 1.0 and 0.40. These ratios were established for all the mixtures based on trial mixes and this was critical as there is no industry standard at present for AAMs. For the preparation of the AAMs, FA, POFA, and GBFS were utilized. FA, POFA, and GBFS were combined to ascertain the impact of CaO on the geopolymerization reaction and gels formulation. As a source of CaO, the GBFS concentration was maintained between 50 and 70%. GBFS contents were ranged from 50 to 70% for the replacement of FA and POFA by GBFS of high volume. Blends with significant volumes of FA, like 50%, were not used in the control mixture in this work. Moreover, for all the mixtures, the NS: NH ratio, the NH molarity and the alkali solution modulus [SiO_2:Na_2O (Ms)] were fixed. Table 2 presents the impacts that different GBFS quantities have on CaO levels in AAMs when used as a replacement for FA and POFA. Additionally, fifteen substitution levels were incorporated and used to determine the effects of CaO on the overall geopolymerization reaction. The findings revealed that with the rise of GBFS levels, CaO contents were improved (Fig. 3). Additionally, CaO content was raised from 19.2 to 37.8% when FA was replaced by GBFS from 50 to 70%. On the other hand, the levels of SiO_2 and Al_2O_3 decreased when the GBFS level was increased, although the extent of the reduction varied based on the chemical composition.

Table 1
Chemical compositions of FA, POFA, and GBFS obtained using XRF test.

Materials	FA	POFA	GBFS
SiO_2	57.20	64.20	30.8
Al_2O_3	28.81	4.25	10.9
Fe_2O_3	3.67	3.13	0.64
CaO	5.16	10.20	51.8
MgO	1.48	5.90	4.57
K_2O	0.94	8.64	0.36
Na_2O	0.08	0.10	0.45
SO_3	0.10	0.09	0.06
LOI	0.12	1.73	0.22
SiO_2: Al_2O_3	1.98	15.11	2.82
CaO: SiO_2	0.09	0.16	1.68
CaO: Al_2O_3	0.18	2.4	4.75

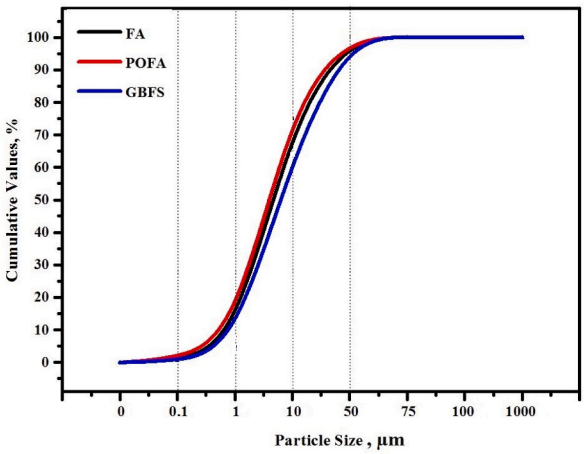

Fig. 1. Particles sizes of FA, POFA and GBFS.

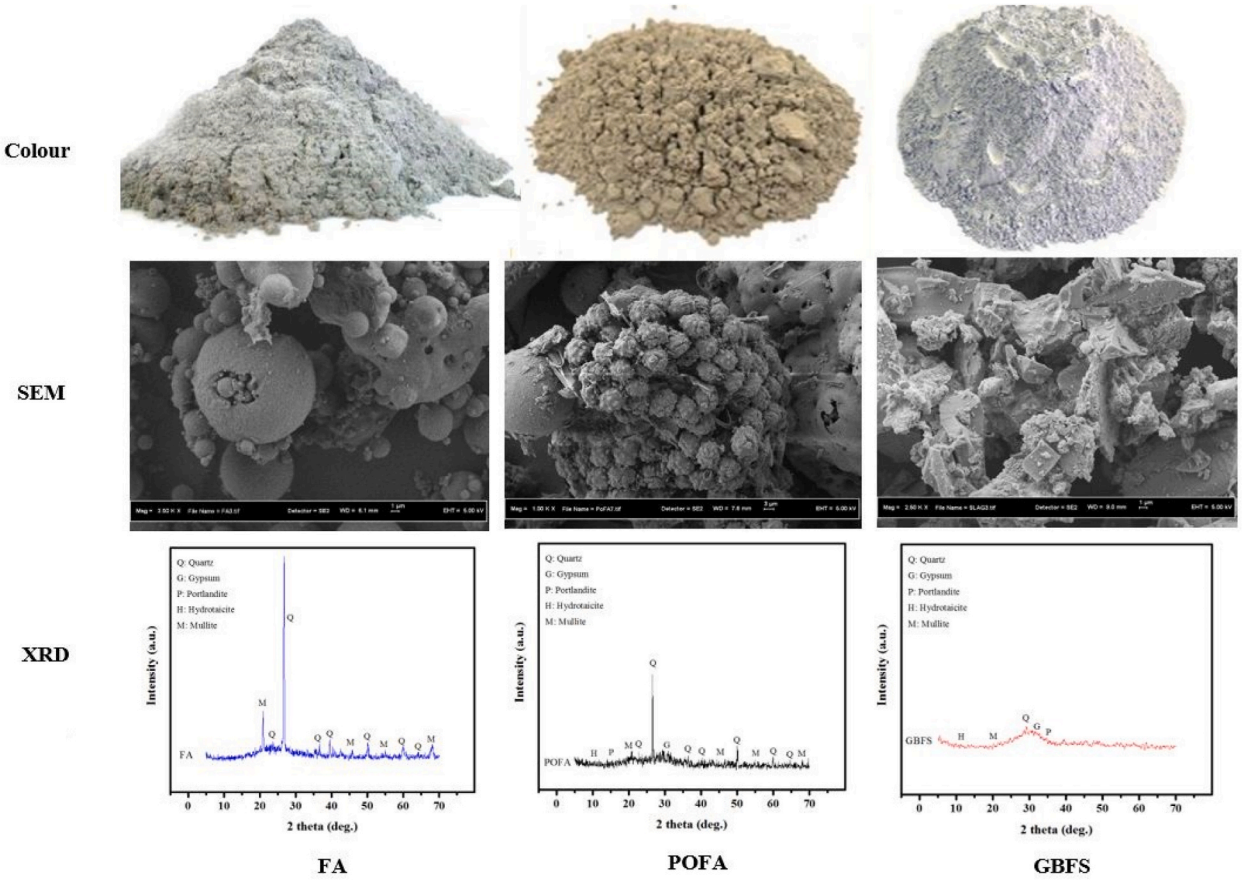

Fig. 2. Mineral properties of binder materials included FA, POFA and GBFS.

2.3. Test procedure

Based on guidelines proposed by the ASTM C109 [27], the CS test was conducted on the AAMs after 1, 3, 7, 28, 56, 90, 180 and 360 days. For each age, three samples were evaluated, and the samples were properly positioned after preparation in accordance with the upper and lower metal bearing plate. AAMs were placed at a fixed loading rate of 2.5 kN/s. The density and CS of AAMs were obtained automatically depending on their weights and sizes. Following to ASTM C666 (−17 to 5 °C) [28], cubic specimens of size (50 m × 50

Table 2
Mix design of FA and POFA based AAMs incorporating high volume GBFS.

Group	Mix	Details of mix designs					
		GBFS	FA	POFA	SiO_2:Al_2O_3	CaO:SiO_2	CaO:Al_2O_3
A	S1	50	50	0	2.22	0.65	1.43
	S2		40	10	2.57	0.65	1.66
	S3		30	20	3.04	0.65	1.97
	S4		20	30	3.68	0.65	2.39
	S5		10	40	4.65	0.65	3.03
	S6		0	50	6.25	0.65	4.07
B	S7	60	40	0	2.29	0.80	1.83
	S8		30	10	2.69	0.80	2.15
	S9		20	20	3.25	0.79	2.59
	S10		10	30	4.06	0.79	3.23
	S11		0	40	5.35	0.79	4.25
C	S12	70	30	0	2.38	0.97	2.32
	S13		20	10	2.85	0.97	2.77
	S14		10	20	3.53	0.96	3.41
	S15		0	30	4.57	0.96	4.41

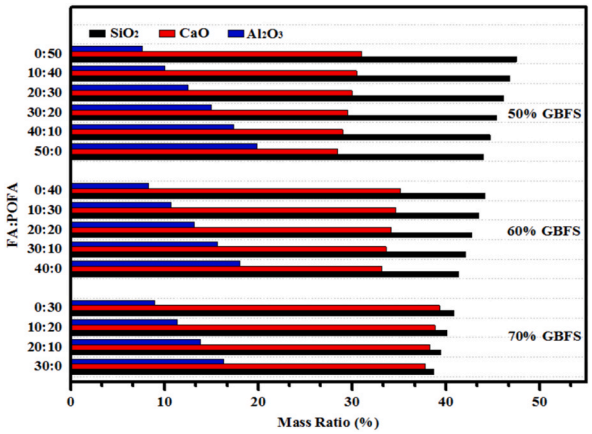

Fig. 3. Impact of high volume GBFS incorporating FA and POFA on SiO_2, CaO and Al_2O_3 content.

mm × 50 mm) were cured for 28 days and then utilized to evaluate their resistance against a total of 300 freezing-thawing cycles. As Method A was better compared to B, the former was utilized in this experiment. After curing the specimens for 28 days they were left to thaw at ambient condition in order to determine the ultrasonic pulse velocity (UPV) and mass. AAMs were immersed in water and a timer was used to control the temperature and achieve each freezing-thawing cycle. A qualitative examination was also performed to determine weight reduction, UPV, and residual compressive strength. In turn, this enabled the effectiveness of AAMs to be assessed. Additionally, AAMs length changes and dynamic modulus were recorded at every 50 cycles for a total of 300 cycles.

According to IS 1237–1980, the abrasion resistance of proposed alkali-activated mortars were evaluated at 1, 3, and 28 days of curing age. Mortar specimens with size (50 × 50 × 50) mm were adopted for this purpose. Firstly, the proposed mortar specimen placed in the machine then the machine rotated at 30 rpm and load of 300 N was applied. The sieved river sand is continuously fed back into the grinding path so that it remained uniformly distributed in the track corresponding to the width of the test mortar specimen. The specimens were tested for 1 h and the reading of weight were taken each 15 min. Then the grind depth was calculated using following formula:

$$I = \frac{(Wx - Wy) \times Vy}{Wy \times Ay} \quad [1]$$

Where.

I: grind depth, mm
Wx: initial weight of proposed mortar cube before the test, gram.
Wy: final weight of proposed mortar cub after the abrasion test, gram.
Vx: initial volume of proposed mortar cube before the test, mm^3.
Ax: The surface area of proposed mortar cube, mm^2.

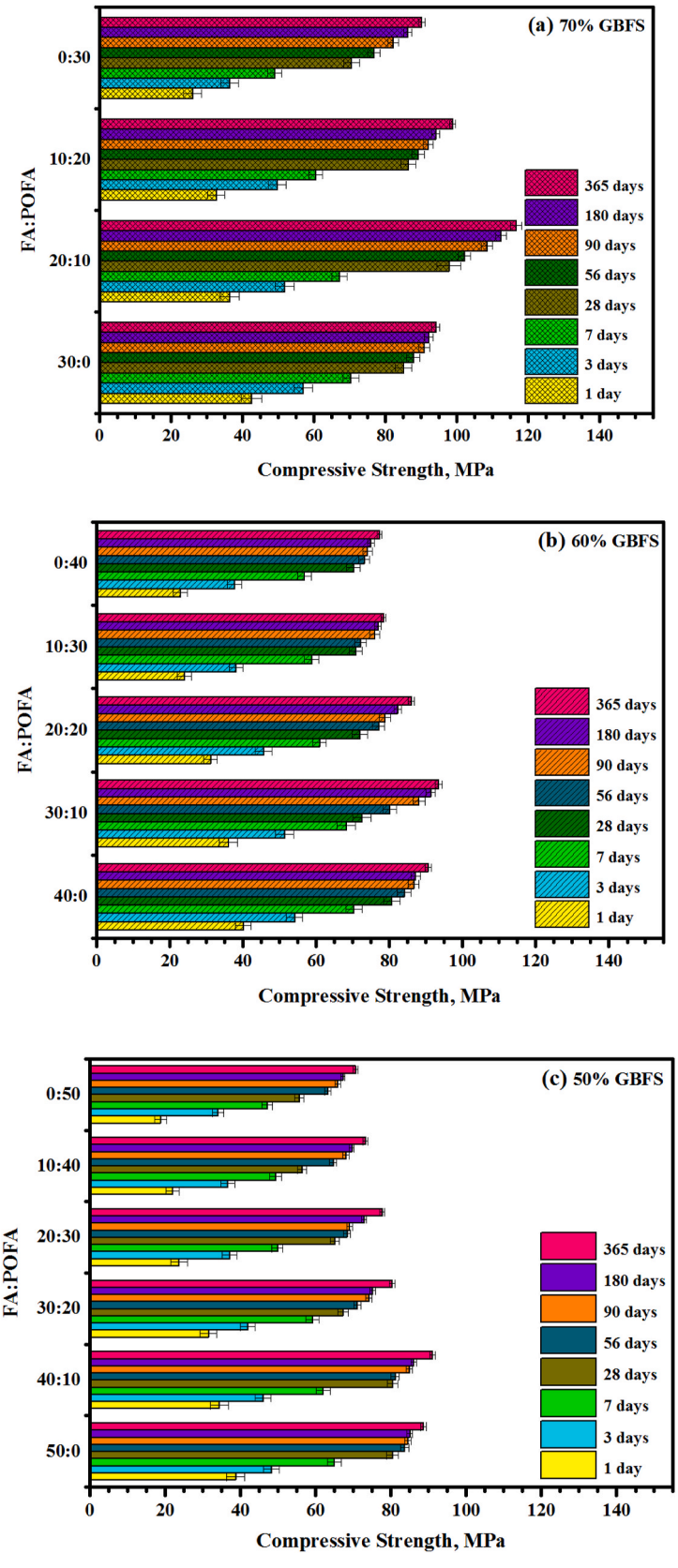

(caption on next page)

Fig. 4. CS development of AMMs made at various FA and POFA level with GBFS contents of (a) 70% (b) 60% (c) 50%.

Following ASTM C642, water absorption (WA) test of the proposed AAMs was performed [29]. Then, each mortar cube was cast in size of (50 × 50 × 50) mm and cured at ambient temperature for 28 days then submerged for 24 h in 27 °C water. Mortar 'specimens were hanged to be weighed after being totally submerged in water (Ws). After saturation, the mixes were oven-dried for an extra 24 h at 105 °C and then weighed (Wd). The values of WA (%) of the mixes were calculated thrice via:

$$WA\ (\%) = [(W_s - W_d)/W_d] \times 100 \quad [2]$$

3. Results and discussion

3.1. Mechanical characteristics

Fig. 4 illustrates the influence GBFS incorporation in place of FA and POFA on the CS values of AAMs. An increasing content of GBFS increased the CS performance. AAMs containing high volume of GBFS as substitute to FA (Fig. 4(a–c)) showed an increase in the early strength from 38.7 to 42.5 MPa at 24 h with the increase of GBFS from 50 to 70%, respectively. Similar trend in the development of CS of AAMs was observed after 3, 7, 28, 56, 90, 180 and 360 days. The CS values of AAMs were 80.5, 80.7 and 85.1 MPa after 28 days, and 88.7, 90.6 and 94.1 MPa after 360 days for GBFS contents of 50, 60 and 70%, respectively. The CS gain of mixes from the final strength at high volume of GBFS was 45, 61, 75 and 90% at 1, 3, 7 and 28 days, respectively.

Fig. 4(a–c) shows the influence of increasing GBFS level as replacement to POFA on the CS development of the AAM specimens that was directly proportional to the increase of GBFS level. The early strength after 24 h was increased with the raising content of GBFS and reduction of the POFA level. The values of CS were 18.7, 22.9 and 26 MPa for the corresponding GBFS level of 50, 60 and 70%. The values of CS revealed similar trend at other ages. The values of CS were 55.6, 70.2 and 70.5 MPa after 28 days, and 70.6, 77.3 and 90.1 MPa after 360 days for the mixes designed with the corresponding GBFS level of 50, 60 and 70%. The specimens prepared with high volume GBFS as replacement of POFA displayed the CS gain from the final CS of 29, 40, 54 and 78% after 1, 3, 7 and 28 days, respectively.

It is established that the amorphous and granular structures of GBFS composed of SiO_2, CaO, and Al_2O_3 (Fig. 3) had high calcium oxide (51.8%) content, facilitating the formation of *C*–S–H gel as major reaction products with CaO to SiO_2 ratio of 1.68 [30]. This *C*–S–H gel could improve the CS of the mortars [30–32]. Kumar et al. [33] demonstrated that the dissolution and precipitation of *C*–S–H gel is dominant at the ambient condition because of the alkaline-activation of GBFS. The generation of cementitious *C*–S–H gels was mainly responsible for the improvement of setting time and CS of the mixes. Al-Majidi et al. [34] examined the effect of GBFS content on the CS development of mortars at different curing regime and ages wherein an increase in the GBFS contents was found to enhance the early ages CS of AAMs. Kumar et al. [35] have examined the effect GBFS content on the AAM matrix and stated that by increasing the GBFS level, the CS and flexural strength (FS) of the mixes can be improved. The inclusion of GBFS was shown to accelerate the hydration reaction, thus forming more *C*–S–H gels [36] and enhancing the strength performance of the mortars.

Three mechanisms were proposed to explain the influence gels formulation by GBFS content. The 1st mechanism involved the improved CS to a greater rate of *C*–S–H gel formulation because of the addition of dissolved CaO from GBFS surfaces [33,37]. Furthermore, a higher rate of *C*–S–H formation due to the existence of CaO may create water shortage in the mortar, increasing its alkalinity to dissolve the existing Al_2O_3–SiO_2 at higher rate [20,38]. The 2nd process was related to the alkali activated products formation of GBFS that are usually predominated by *C*-A-*S*-H gels. The presence of aluminum ions can lead stronger polymerization and considerable cross-linking among *C*–S–H chains [39]. The creation of *N*-A-*S*-H was claimed to be the last mechanism that can appreciable improve the CS of mortars. Certainly, *N*-A-*S*-H gels being a negligible secondary product that coexist in the composition range of the major *C*–S–H types gel [40], improving the gels compactness, and reducing the total pore volume thereby improving the CS values of the mortars [41].

The results (Fig. 4(a, b) and c) clearly displayed that the AAMs made with high volume of GBFS and FA presented better CS than those prepared with GBFS and POFA. After 28 days, a compressive strength value of 80.5, 80.7 and 85.1 MPa were achieved for AAM matrix containing GBFS and FA. However, AAM matrix containing GBFS and POFA revealed a compressive strength value of 55.6, 70.2 and 70.5 MPa that was lesser compared to the reported mixes. The effect POFA on early CS can clearly be seen in Fig. 4 (c). The CS gain of the AAM after 24 h was reduced to 29% and 45% for the blend containing POFA and FA, respectively. Similar trend of CS was observed after 3, 7, 28, 56 and 90 days and still the strength gain with FA was higher than the one with POFA. The higher ratio of silicate to aluminium (6.25) was achieved for the matrix with 50% of POFA compared to a ratio of 2.2 for the matrix containing 50% of FA, which reduced the strength from 80.5 to 55.6 MPa at 28 days. Ranjbar et al. [42] found that an increase in the ratio of SiO_2 to Al_2O_3 produce negative effect on the CS performance of proposed binders. In addition, a decrease in the Al_2O_3 level with the increase of POFA percentage showed a considerable effect on the formation of *C*-A-*S*-H gels, lowering the CS values [43,44] and slowing down the reaction rate of mortars.

In each level of high volume GBFS (50, 60 and 70%), the influence of POFA as FA substitution on the CS development of AAMs at early and late ages were assessed (Fig. 4). The impact of POFA replaced to FA on the CS values of mixes designed with 60 and 50% of GBFS (Fig. 4 (b) and (c)) showed that an increase in the POFA level could lower the early ages CS. FA replacement by 10% POFA in AAMs containing 60 and 50% GBFS after 90 days has enhanced the compressive strength (88.1 and 84.8 MPa) compared to 86.6 and

84.4 MPa. Ariffin et al. [45] showed that low level of Al_2O_3 was responsible for the reduced CS, wherein incomplete geopolymerization due to higher dissolution of Al_2O_3 at early age caused such reduction. For 70% GBFS containing AAMs a reduction in the ratio of FA: POFA from 30:0 to 0:30 have negatively affected the early strength after 1, 3 and 7 days (Fig. 4 (a)). The values of CS for mortars were 42.5, 36.5, 32.7 and 26 MPa for the corresponding POFA contents of 0–10, 20 and 30%. In short, low content of Al_2O_3 was responsible for the drop of early CS of AAMs [46,47]. After 28 days, the CS values of AAMs were enhanced from 85.1 to 86.5 MPa with the increase of POFA contents from 0 to 20%, respectively). The rise of POFA level to 30% could reduce the CS to 70.5 MPa.

Fig. 5 shows the influence of the proportions of SiO_2 to Al_2O_3 and CaO to SiO_2 on the CS development of AAMs made with high GBFS of high volume wherein the strength of the mixes was affected significantly with increasing ratios. The improved CS was inversely related to the ratio of SiO_2 to Al_2O_3, achieving an optimal value of 55.6 MPa at a ratio of 6.5. The CS of the mortar was maximum (97 MPa) at 28 days for CaO to SiO_2 ratio of 0.97. SiO_2 to Al_2O_3 ratios of 2.75 and 3.25 could reduce the corresponding CS of mortar after 28 days to 86.4 and 85.1 MPa (Fig. 6). It was demonstrated that as the percentage content of silicate increase and calcium and aluminum level was decreased, the CS of AAMs was reduced.

3.2. XRD analysis

Fig. 7 illustrates the XRD profiles of the designed AAMs composed of high GBFS contents. Three levels of GBFS were replaced of FA with 50, 60 and 70% specimens were prepared. The results show the dense gels of Gismondine ($CaAl_2Si_2O_8{\cdot}4(H_2O)$) and Zeolite (Na or K or Ca–$AlSi_3O_8$) peaks intensity between 20° and 28° were increased as the GBFS content increase, at 29.9° the intensity of Albite ($NaAlSi_3O_8$) peak also observed increase as the content of GBFS increased. When the GBFS level in the mixes was increased from 50 to 70% the XRD pattern showed new peak at 24° and Gismondine ($CaAl_2Si_2O_8{\cdot}4(H_2O)$) peak was replaced with the quartz. With 70% GBFS, Zeolite peak was replaced by Mullite at 16°. This increase in the GBFS level led to the formation of more dense *C*–S–H gels. The presence of Gismondine and Alibte in the AAMs was responsible for the enhancement of strength and surface morphology of the mixes.

Fig. 8 displays the influence of high level GBFS replaced POFA at 50, 60 and 70%. An increasing amount of GBFS has enhanced the dense gel peaks intensity and reduced the quartz peak intensity. AAMs with increasing content of GBFS (60 and 70%) and decreasing content of POFA (40 and 30%) revealed new peaks such as Zeolite, Albite and Gismondine beside the dense amorphous N, *C*-A-*S*-H gel that significantly improved the strength performance. This dense gel could improve the AAMs surface structure and the strength from 63.2 to 73.1 and 76.9 MPa.

Fig. 9 shows the XRD pattern of AAMs containing 70% of GBFS and POFA as FA replacement. The gel peaks verified the presence of calcium in chemical composite such as Albite, and Gismondine for 0 and 10% POFA replaced FA. The Albite peak at 31° for 10% POFA showed higher intensity and lower width than similar peak at 0% POFA, implying that the dense gels product in 10% POFA was higher than 0%. This explained the improvement of mortar compressive strength to 97.7 MPa compared to 85.1 MPa recorded with 0% FOFA. When the content of POFA replaced FA raised to 20% some of the peaks were altered, where Zeolite peak replaced the mullite at 16°, leading to a reduced strength of alkali-activated specimens from 97.7 to 86.4 MPa.

Fig. 10 shows XRD of binder containing 50% of GBFS and POFA as FA replacement. Six levels of POFA replaced FA mixes were prepared and examined at 28 days of age. The specimens started with 0% of POFA replaced FA then gradually increased to 10, 20, 30, 40 and 50%. As the content of POFA was increased the quartz peak intensity at 28 and 21° was also improved. The Gismondine peak at 28° for the mix containing 0% of POFA showed the peak of quartz replacement and shift of Gismondine peak to 27.8°. An increase in the ratio of POFA replaced FA led to a raise in the unreacted SiO_2 and thus controlled the dense gels product. This in turn lowered the CS of the mortars from 80.5 to 55.6 MPa with the corresponding increasing POFA level from 0 to 50%.

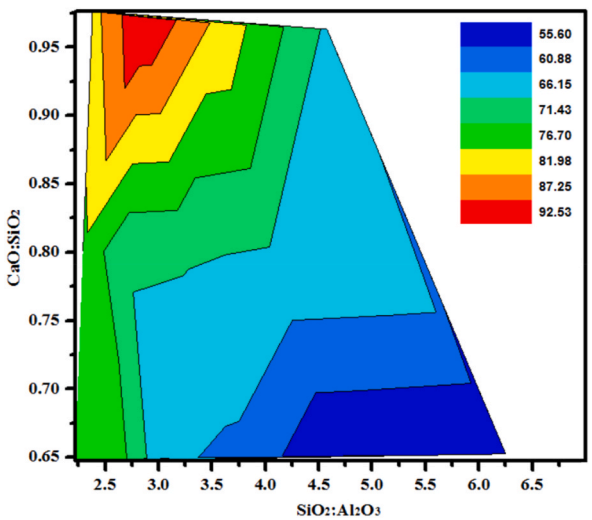

Fig. 5. Influence of SiO_2 to Al_2O_3 and CaO to SiO_2 ratios variation on the CS of mixes.

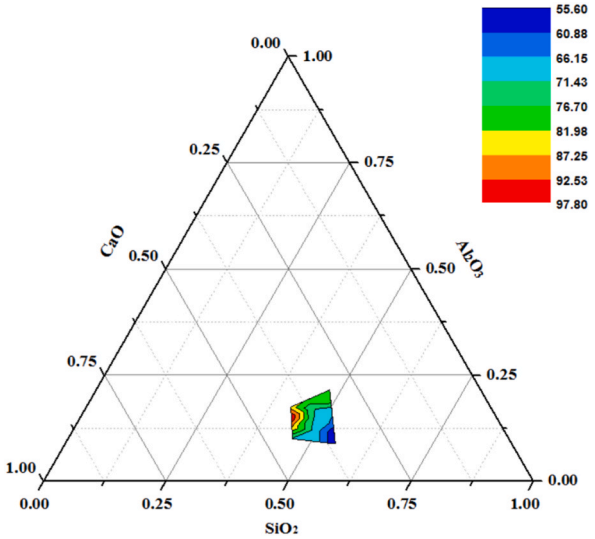

Fig. 6. SiO_2, Al_2O_3 and CaO contents dependent changes in the CS of AAMs.

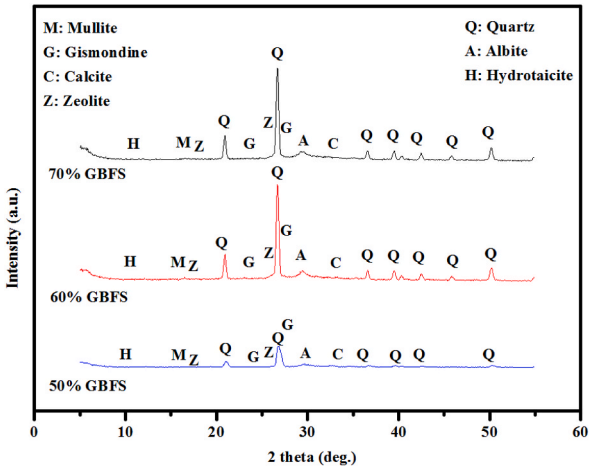

Fig. 7. XRD profiles of AAMs composed of 50, 60 and 70% GBFS at 28 days of curing.

3.2.1. *Scanning electronic microscopy (SEM)*

Three levels of high volume GBFS specimens were prepared for comparing the microstructures of AAMs containing FA. Fig. 11 presents the SEM results for 50, 60 and 70% GBFS at 28 days. As seen in the SEM images the dense gel was increased with increasing content of GBFS. Generally, with the increase of GBFS level more *C*–S–H gel was produced, enhancing the microstructures of the specimens [5]. Fig. 11 (a) shows the SEM image of AAM containing 70% GBFS. Most of the sample surface appeared due to the existence of little amount of partially-reacted and unreacted grains. Fig. 11 (b) and (c) illustrates the microstructure of AAM with 60 and 50% of GBFS, respectively. These grains were increased with the decrease of GBFS content and showed a less compact and highly porous surface than the one having 70% of GBFS content.

Fig. 12 displays the SEM micrographs of mortars containing 70% of GBFS. The results of SEM showed that the substitution of FA by 10% of POFA has enhanced the microstructure of alkali-activated matrix wherein the surface revealed more compactness and less porosity than the mixes containing 0 and 20% of POFA. Mortar made 20% of POFA showed more particles that were reacted partially or not reacted at all. These particles were rarely observed on the AAMs surface at low amount of POFA as shown in Fig. 12 (a) and (b). On [8], the authors reported that the CS and surface morphology of design mortar significantly depends majorly on the SiO_2 to Al_2O_3 ratio. It was further acknowledged that Si to Al ratio above 3.50 can negatively influence the CS performance of mortars [48].

3.3. *FTIR spectra*

Fig. 13 shows the FTIR spectrum of the designed mixes containing high volume GBFS. Table 3 illustrates the FTIR band locations

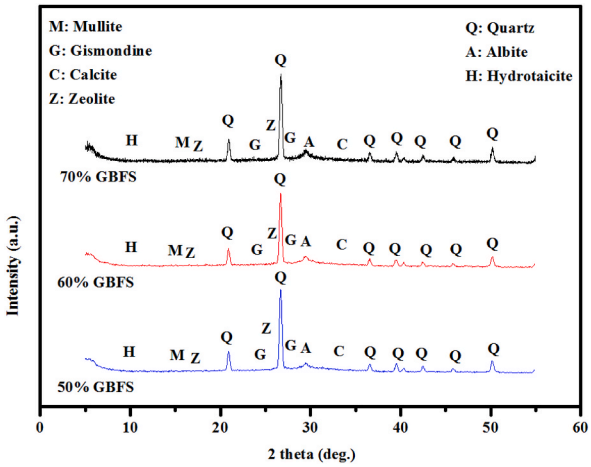

Fig. 8. XRD profiles of AAMs made from 50, 60 and 70% of GBFS at 28 days.

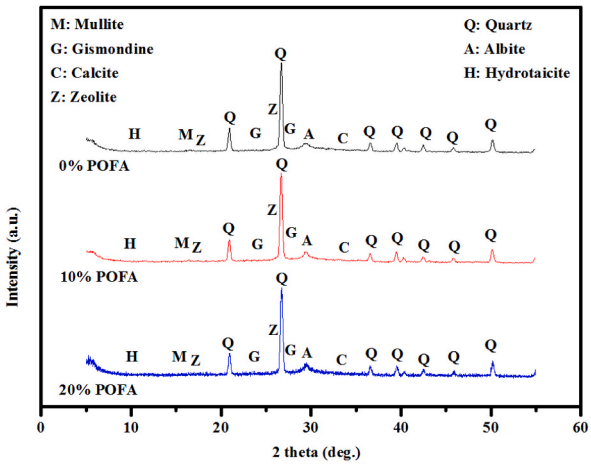

Fig. 9. XRD profiles of AAMs composed of 70% of GBFS at different POFA content as FA replacement.

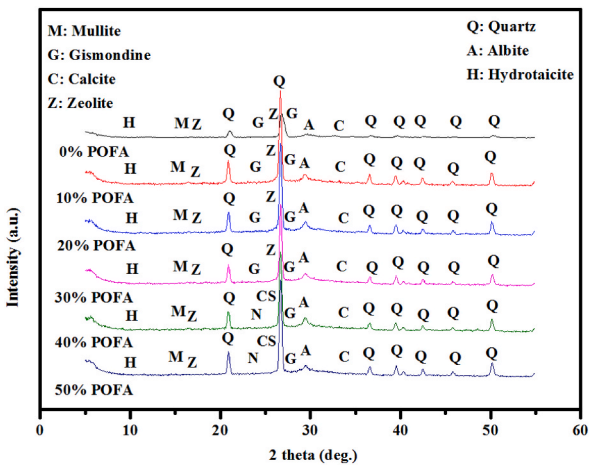

Fig. 10. XRD analysis of AAMs made with 50% of GBFS at various levels of POFA as FA replacement.

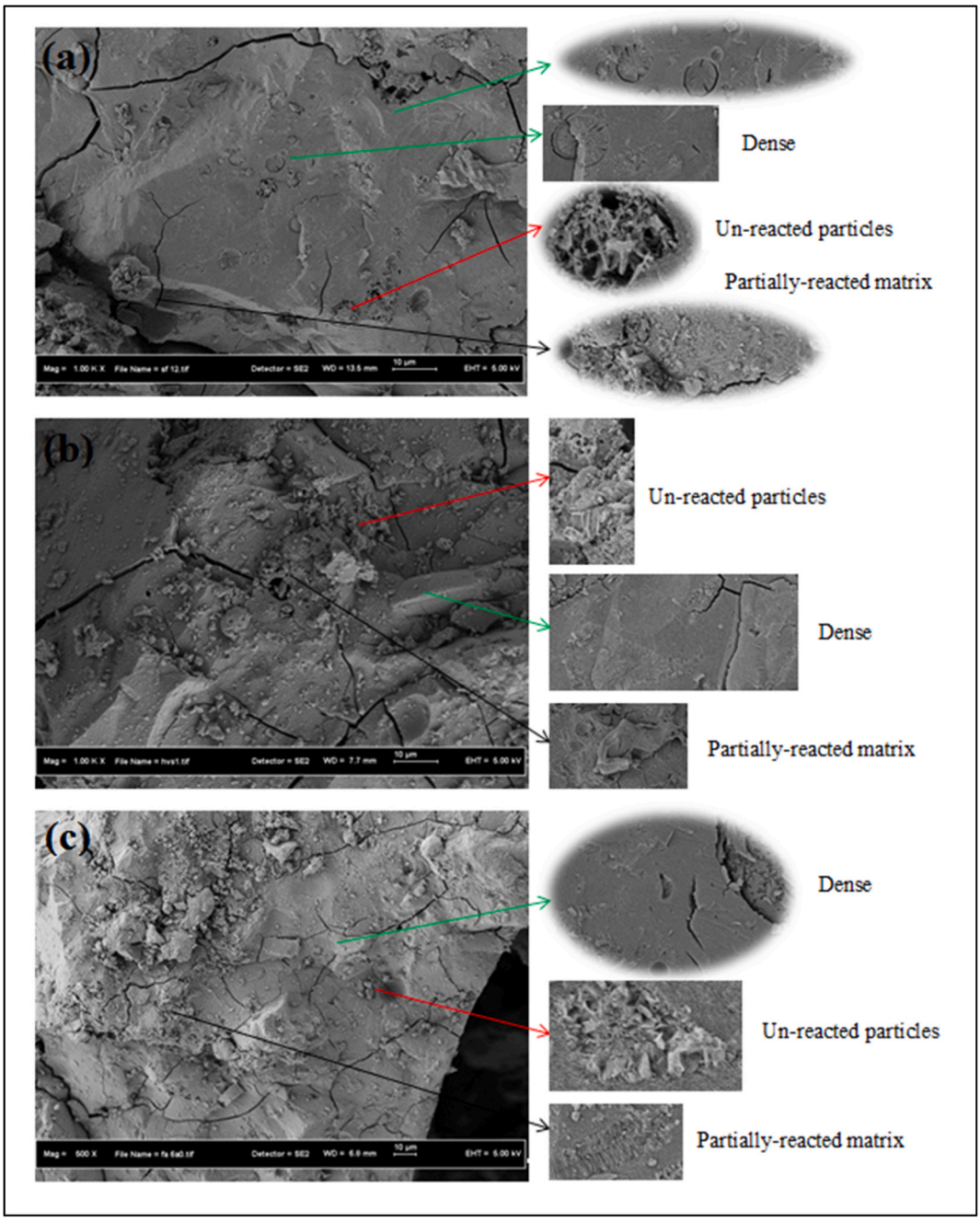

Fig. 11. Impact of high level GBFS on the surface morphology of FA incorporated AAMs (a) 70% GBFS (b) 60% GBFS (c) 50% GBFS.

and bond vibration. The results of GBFS replaced FA at 50, 60 and 70% indicted to the bands of 50% GBFS at 755.3, 871.5 and 945.6 cm^{-1} were decreased to 743.7, 865.6 and 945.1 cm^{-1} with 60% and 730.1, 865.1 and 944.4 cm^{-1} with 70% of GBFS containing mixes, respectively. The reduction in bands frequency was related to the increase of GPMs CS from 80.5 to 80.7–85.1 MPa. Furthermore, creation of AlO_4, *C*–S–H and *C*–N-A-*S*-H showed inverse relation to the band wavenumber. The bands at lower wavenumber implied the dissolution more silica thereby forming higher amount of AlO_4, *C*–S–H and *C*–N-A-*S*-H [49]. Mortars made with the replacement of POFA by GBFS at 50, 60 and 70% showed a decrease in the band frequency with the increase of GBFS contents. This observation was attributed to the creation of more *C*–S–H and *C*–N-A-*S*-H gels. The low strength of AAMs made with POFA and without FA inclusion was explained using FTIR analysis. With increasing POFA level the amount of Al was reduced, allowing the dissolution of silicate and lead which in turn lowered AlO_4, *C*–S–H and *C*–N-A-*S*-H products as evidenced from the band position of POFA added mixes (Table 2) than FA-incorporated ones. For mixes containing 50% of GBFS, the effects of POFA substituted FA was also evaluated using FTIR spectral

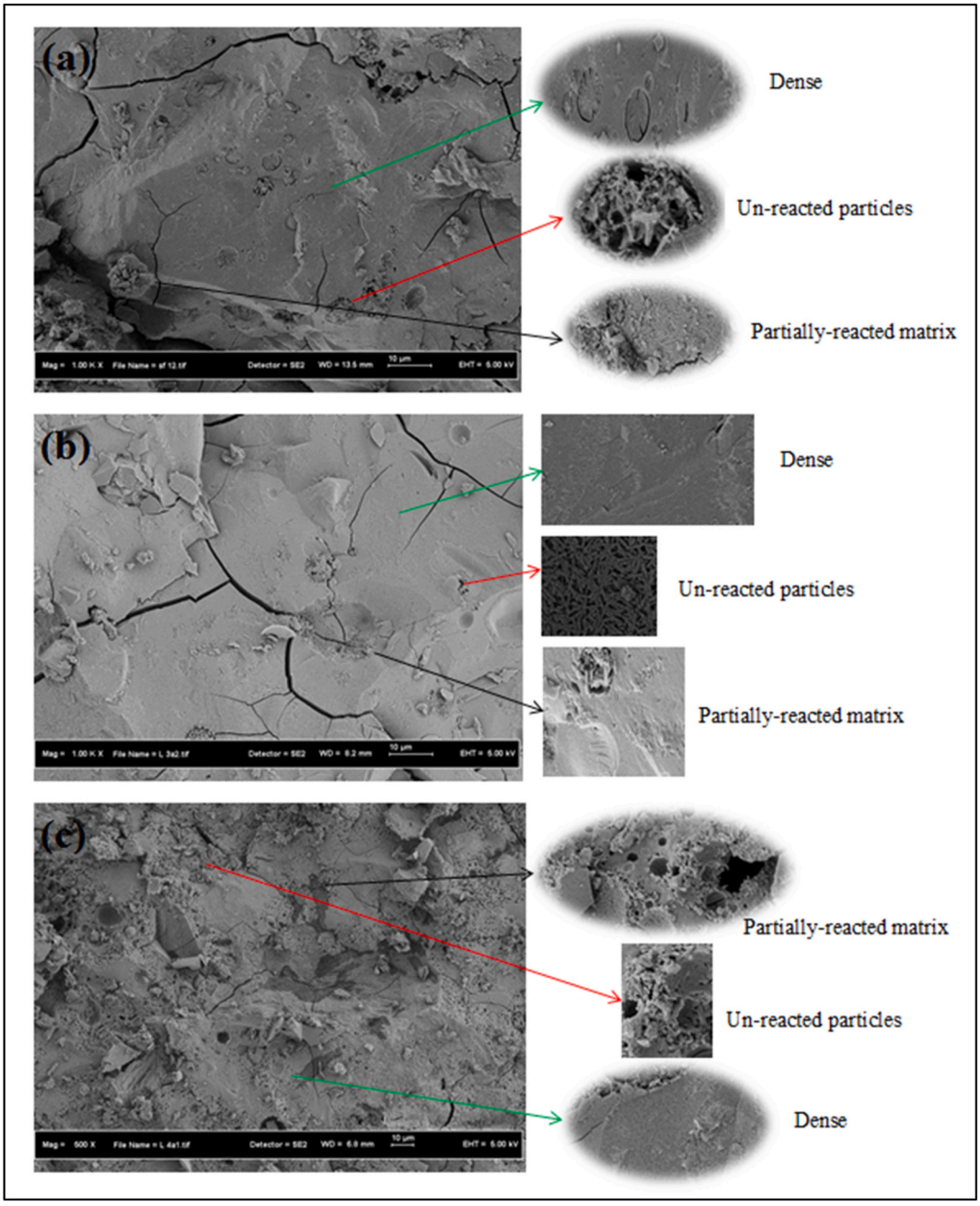

Fig. 12. SEM images of 70% of GBFS based AAMs incorporating various level of POFA as FA replacement (a) 0% POFA (b) 10% POFA (c) 20% POFA.

analysis. The band position of *Si–O*–Al was improved with the raise of POFA contents. In addition, the proposed mortar CS was reduced from 80.5 to 65.1 to 55.6 MPa at 0, 30 and 50% POFA content.

3.4. Freezing-thawing resistance

The residual CS, internal frost damages, and surface scaling of the proposed mortars were examined as a function of high volume GBFS in the mixes wherein the mixes were subjected to freezing and thawing (300 cycles) at 28 days. The influence of high volume GBFS (50, 60 and 70%) in place of FA for the AMMs durability was evaluated (Figs. 14–16). The residual CS of the mixes were enhanced from 48.6 to 69.6 MPa with the increase GBFS level from 50 to 70% (Fig. 14). The values of internal frost damages were increased with the increase of cycles number, the reduction in internal damage was decreased with raise GBFS level as shown in

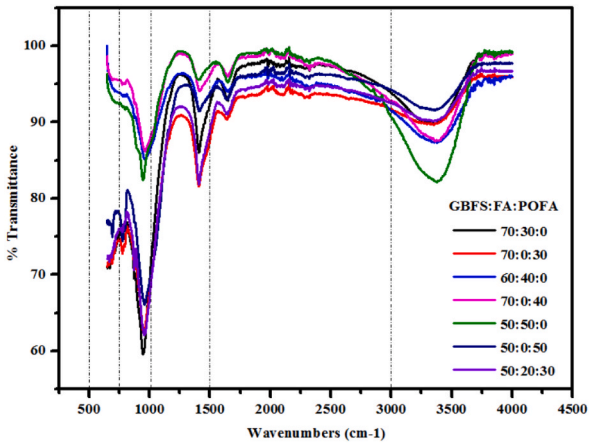

Fig. 13. Effect of high level of GBFS on FTIR spectra of AAMs.

Table 3
Effect of high level of GBFS on ternary blended alkali-activated' FTIR results.

Mix			*Fc* (MPa)	FTIR band position (cm^{-1}) and assignment				
GBFS:FA:POFA	Si/Al	Ca/Si		Al–O	*Si*–O	AlO_4	*C*–S–H	*C*-(N)-A-*S*-H
70:30:0	2.38	0.97	85.09	651.6	683.5	730.1	865.1	944.4
70:0:30	4.57	0.96	70.53	668.9	690.4	795.1	870.4	954.4
60:40:0	2.29	0.80	80.68	664.9	690.1	743.2	865.6	945.1
60:0:40	5.35	0.79	70.22	665.4	691.5	796.9	871.5	955.6
50:50:0	2.22	0.65	80.46	671.7	690.9	755.3	871.7	945.6
50:20:30	3.68	0.65	65.14	663.7	691.5	777.2	871.9	956.1
50:0:50	6.25	0.65	55.64	652.5	691.9	805.7	872.1	956.9

ultrasonic pulse velocity in Fig. 15 Residual weight and surface scaling of alkali-activated specimens trend to decrease with increasing GBFS content and recorded residual weight 98.6, 99.2 and 99.4% with 50, 60 and 70% GBFS respectively as depicted in Fig. 16. The high durability of high volume GBFS replaced FA can clearly observe from residual weight results and surface deterioration was shown in Fig. 17. With the increase of GBFS level, the porosities of AAMs were lowered with the refinement of pores GBFS content, contributing to the lowering of ice development [50]. Meanwhile, the pores the mixes became more disjointed and reduced the capillary transports of exterior liquid into the pores of mortars during the freezing-thawing cycles. Consequently, less ice was grown that is proposed to be the main scaling process governed by the cryogenic suction of surface liquids under the freezing stage [51].

The effects of high level GBFS as substitute to POFA of 50, 60 and 70% on the residual CS and surface scaling features of the mixes evaluated as shown in Figs. 18–20, respectively. The results showed inverse relation between loss of strength and GBFS content, wherein the loss of strength was reduced with the increase of GBFS level. The residual CS of mortars was 20.1, 34.1 and 36.2 MPa at 50,

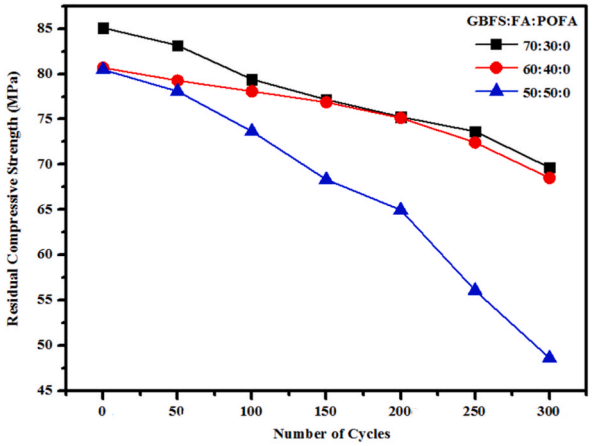

Fig. 14. GBFS contents dependent residual CS of AAMs.

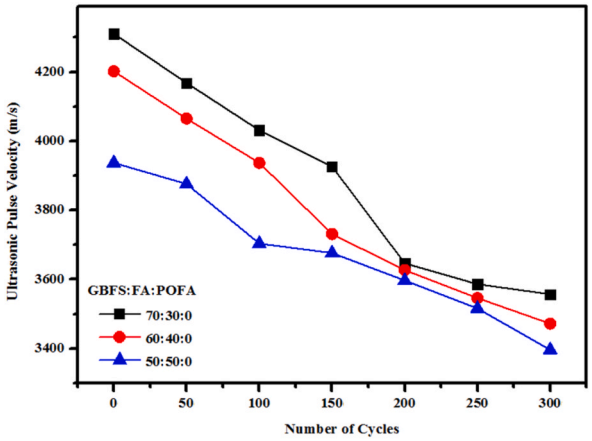

Fig. 15. GBFS contents dependent UPV of AAMs.

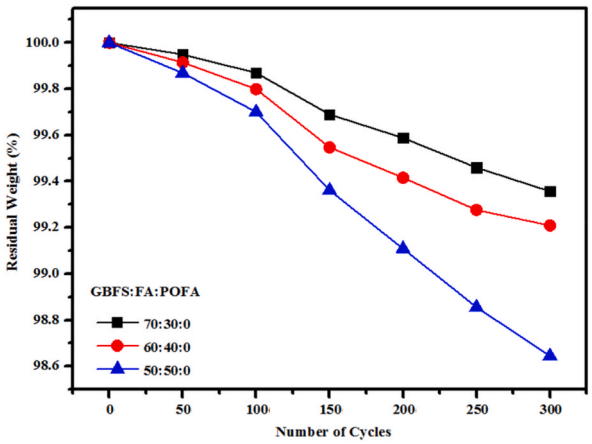

Fig. 16. GBFS contents dependent residual weight of AAMs.

60 and 70% of GBFS contents (Fig. 18). The results of internal frost damage and lose weight are decreased with increasing GBFS content as shown in Fig. 19. Fig. 20 depicts the level of deterioration of the specimens wherein the damage was decreased with the increase of GBFS content.

The impact of various POFA level as FA replacement on the residual CS of the mortars containing 70% of GBFS was evaluated (Fig. 21). The replacement of FA by 10% POFA was observed to enhance the strength and durability properties of the AAMs as explained before. Lower contents of voids could contribute to an increase in the resistance of specimens to freeze/thaw cycles. Increase of POFA content higher than 10% led to more porous structure of the mortar with lower resistance. An increase in the POFA level could lower the residual CS of AAMs to 36.1 MPa for 30% of POFA compared to 69.7 MPa for 0% of POFA after 300 cycles. Similar trend of was observed with residual weight results, where the weight loss was increased with raising POFA level more than 10% as presented in Fig. 22.

Figs. 23 and 24 show the impact of POFA as FA substitution on the residual CS and weight for 50% of GBFS containing specimens. It was observed that the loss strength and weight was directly proportional to the POFA content. When the POFA level was increased to 50% the strength of the mortar was reduced to 20.1 with loss weight above 5% after 300 cycles than 48.6 MPa and loss of weight was below 98% for mortar made with 0% of POFA. When the freeze/thaw cycles and POFA level were increased, the damage was mostly observed on the mortars surface and edge (Fig. 25). Furthermore, the higher deterioration was observed for AAMs containing 50% POFA.

3.5. Abrasion resistance (AR)

Fig. 26(a–c) displays the influence of high GBFS level on the abrasion resistance (AR) of AAMs. The AR of mortars showed direct proportionality with the curing age and GBFS content. All the designed mixes revealed higher AR at 28 days than at 1, 3 and 7 days. In addition, the AR values were affected by the variation of GBFS contents, wherein the grinding depths of AAMs were decreased from 1.07 to 0.68 then 0.66 with increasing GBFS content from 50 to 60 and 70% respectively at 28 days. The impact of POFA as FA substitution in the mortars made with 70, 60 and 50% of GBFS was evaluated as shown in Fig. 27 a, b and c respectively. The results

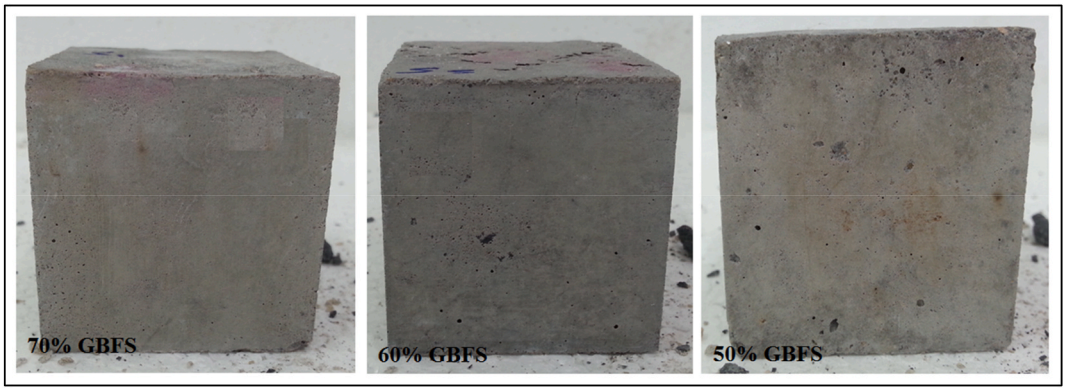

Fig. 17. GBFS contents dependent surface texture weight of AAMs when exposed to 300 freeze/thaw cycles.

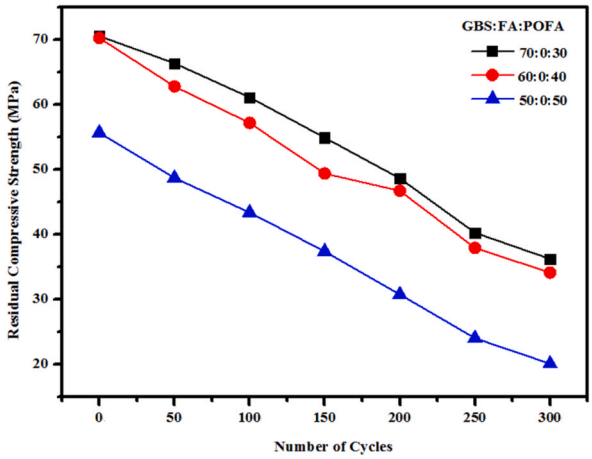

Fig. 18. Impact of high GBFS contents on residual CS of AAMs.

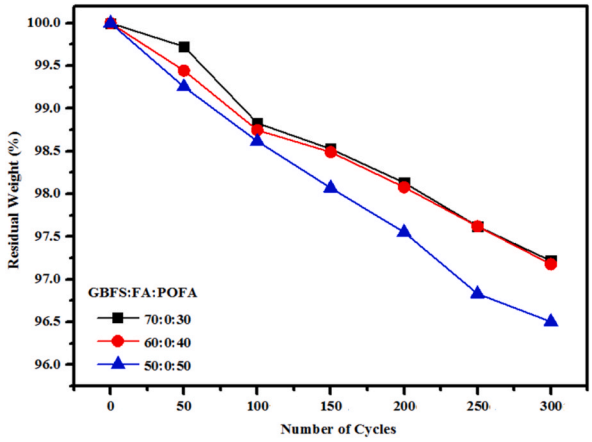

Fig. 19. Impact of GBFS contents on the residual weight of proposed mortars.

indicted to as POFA replaced of FA level increased the abrasion resistance decrease and the grind depth increased from 1.07, 0.68 and 0.66 mm to 1.7, 0.88 and 0.86 mm at 50, 60 and 70% of GBFS specimens. The highest abrasion resistance value was obtained with alkali-activated mixture content 70% of GBFS, 20% of FA and 10% of POFA and recorded value of grind depth 0.61 mm at 28 days. As the strength of the AAMs was enhanced with the increase of GBFS content, the porosity was dropped to low values, improving the AR of the mortars with the increase of GBFS content. The AR in directly proportional with strength value and reduction porosity [52].

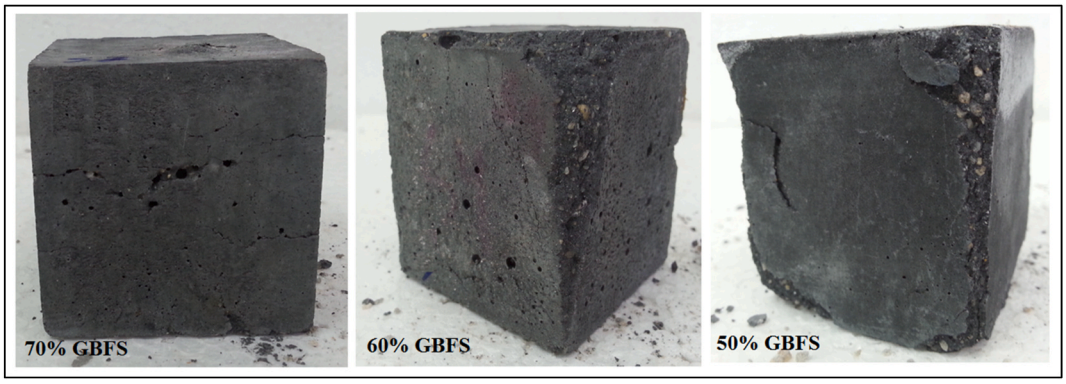

Fig. 20. Impact of high GBFS contents as substitute of POFA on the residual weight of AAMs.

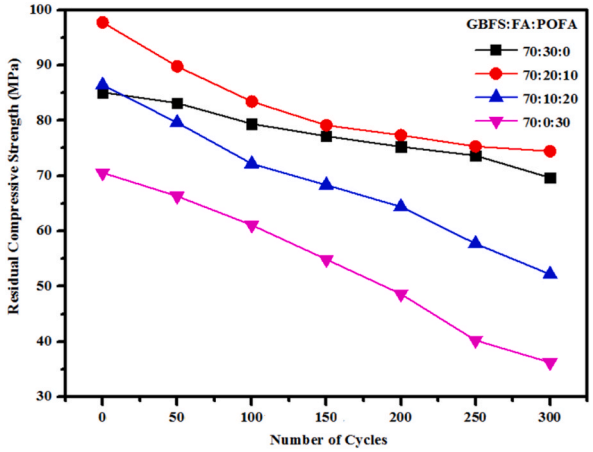

Fig. 21. Residual CS of AAMs containing 70% of GBFS and POFA as FA replacement.

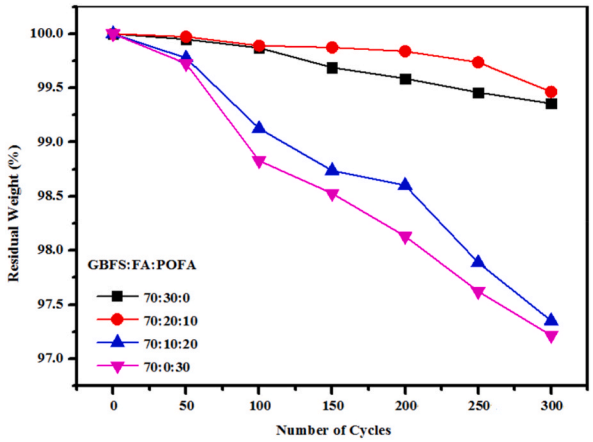

Fig. 22. Residual weight of AAMs containing 70% of GBFS and POFA as FA replacement.

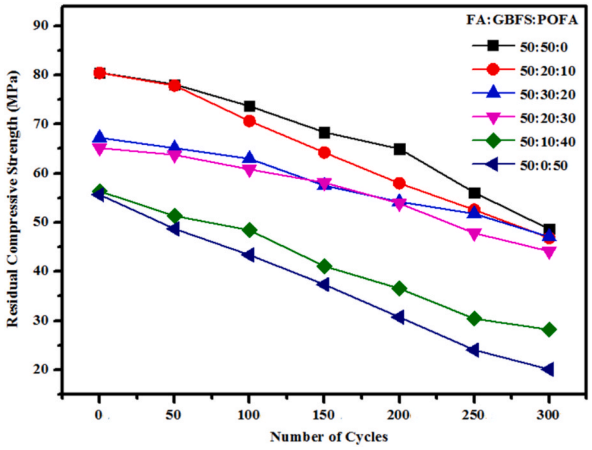

Fig. 23. Impact of POFA as FA replacement on residual CS of AAMs containing 50% of GBFS.

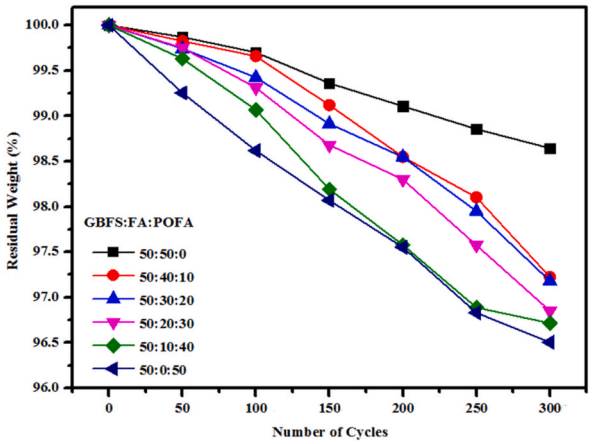

Fig. 24. Residual weight of proposed mortars made with GBFS and POFA of 50% as replacement of FA when exposed to freezing-thawing cycles.

3.6. Resistance of mortars to wet-dry cycles

The deterioration of the wet-dry resistance for AAMs made with high volume of GBFS is shown in Fig. 27. The strength loss of AAMs showed a reciprocal relation to GBFS content. The strength loss value was decreased from 7.7 to 6.9 and 6.8% with raised GBFS level from 50 to 60 and 70%. The weight loss values also affected by GBFS content and the values were decreased with increasing GBFS content. In 70% of GBFS specimens, it was found the values of strength and weight loss in directly proportional with content of POFA replaced FA, the strength loss amount was raised from 6.8 to 6.8, 7.1 and 15.9% with raising POFA content from 0 to 10, 20 and 30% as shown in Fig. 27 (a). Weight loss of mixes was increased from 0.3 to 1.1% with the corresponding rise of POFA contents from 0 to 30% (Fig. 27 (b)). Fig. 27(a–b) illustrates the strength and weight loss of mortars as function of increasing POFA level as substitute to FA in the mortars made with 60 and 50% of GBFS. Mortars containing high volume of GBFS showed the low porosity and high density structures wherein both internal and external damages were lowered, indicating high resistance against the deterioration in wet/dry cycles.

3.7. Water absorption

Fig. 28 shows the water absorption (WA) of high volume GBFS containing AAMs at 28 days. The WA values were decreased with increasing GBFS level replaced of FA or POFA. Water absorption of properties of the proposed mortar was affected significantly by the GBFS to FA ratios wherein the WA values were 7.8, 7.2 and 7.1 for 50, 60 and 70% of GBFS content, respectively. The recorded water absorption values for GBFS replaced POFA with 50, 60 and 70% were 10.4, 9.2 and 8.5%, respectively. In addition, the designed mixes containing high amount of POFA showed enhanced WA than FA containing specimens. The effect of FA replacement by POFA at every GBFS level of high volume was studied. At 50% of GBFS, the POFA replaced FA containing AAMs revealed increasing water absorption values. Substitution of FA by POFA at 0, 10, 20, 30, 40 and 50% revealed water absorption of 7.8, 8.7, 9.2, 10.1, 10.3 and 10.4. Similar

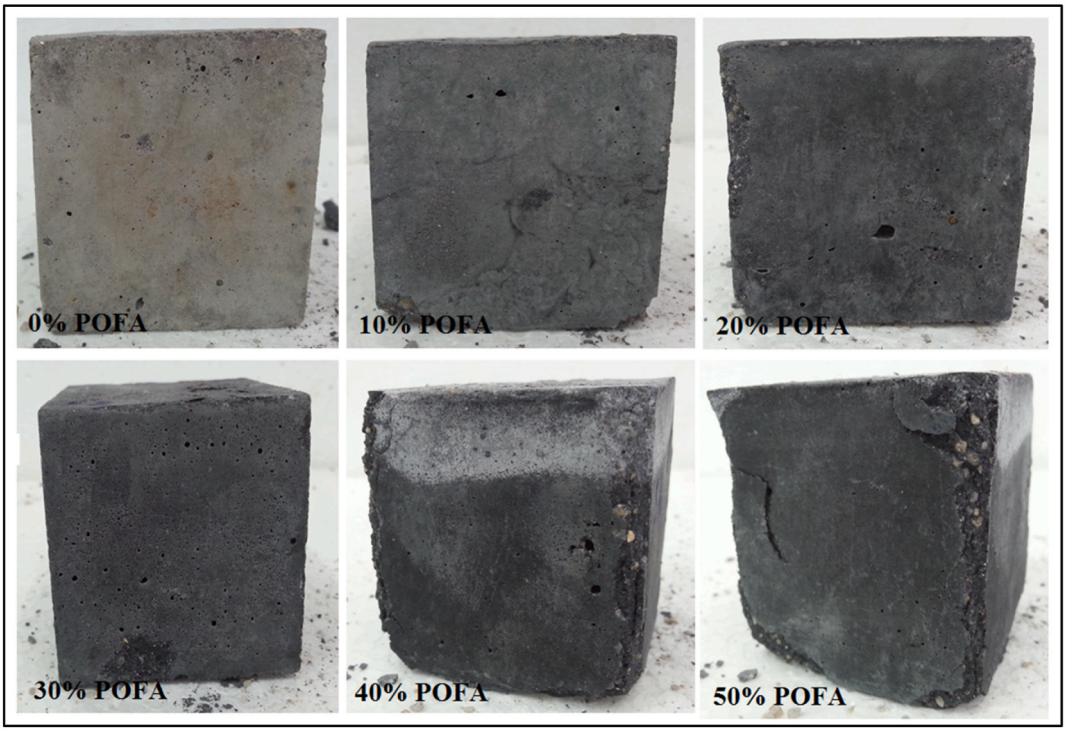

Fig. 25. Surface structures of AAMs made with 50% of GBFS.

trend was found with POFA replaced of FA at 60% GBFS. For 70% GBFS level, POFA replaced FA with 10% caused a reduction in the water absorption from 7.1 to 6.8%. However, as the increase level of POFA replaced FA more than 10% has effect to increase the water absorption and recorded values 7.4 and 8.5% corresponding to 20 and 30% of POFA level. This observation was ascribed to the formation of more dense *C*-A-*S*-H gel with the increase of GBFS, leading to the development of more uniform CS with low WA as explained in section 3.1.

The relationship between WA and CS for the proposed mortars is shown in Fig. 29. The values of WA were significantly dropped, improving the CS of the AAMs. The linear regression technique was used to determine the correlation between the experimentally measured results with $R^2 = 0.74$ following Eq. (3) with signified good confidence for the relation.

$$WA = 0.0979fc + 15.612 \left(R^2 = 0.7439\right) \quad [3]$$

where *WA* is the water absorption of AAM specimens and *fc* is the cube compressive strength.

4. Conclusions

Influence of high volume GBFS (50, 60 and 70%) together with FA and POFA inclusion on the performance of AAMs were determined. GBFS contents dependent strength, abrasion, water absorption, microstructures performance, freeze/thaw resistance, and wet-dry resistance of the proposed AAMs were analyzed. It was concluded that.

i. The compressive strength development of ternary blended based alkali-activated mortar was significantly influenced by high volume GBFS level, where the highest values of strength was observed with higher level GBFS content in the alkali-activated matrix.
ii. AAMs containing FA and POFA produced negative impact on the strength values at early age. The gain of strength for the specimen at 28 days was influenced negatively by the increase of POFA content.
iii. The designed AAMs achieved a gain in the strength between 81 and 94% after 28 days as compared to those after 360 days.
iv. In-depth microstructures analyses using diffractometry, microscopy, and spectroscopy confirmed an appreciable strength improvement of AAMs at high volume of GBFS and low concentration of alkali-solution activation. With the increase of GBFS level more dense *C*–S–H, *C*-A-*S*-H and *N*-A-*S*-H gels were formed that considerably improved the strength performance and durability of the alkali-activated matrix. The increment in gels formulation led to improve the surface morphology of proposed mortar with reduction in pores and non-reactive particles.

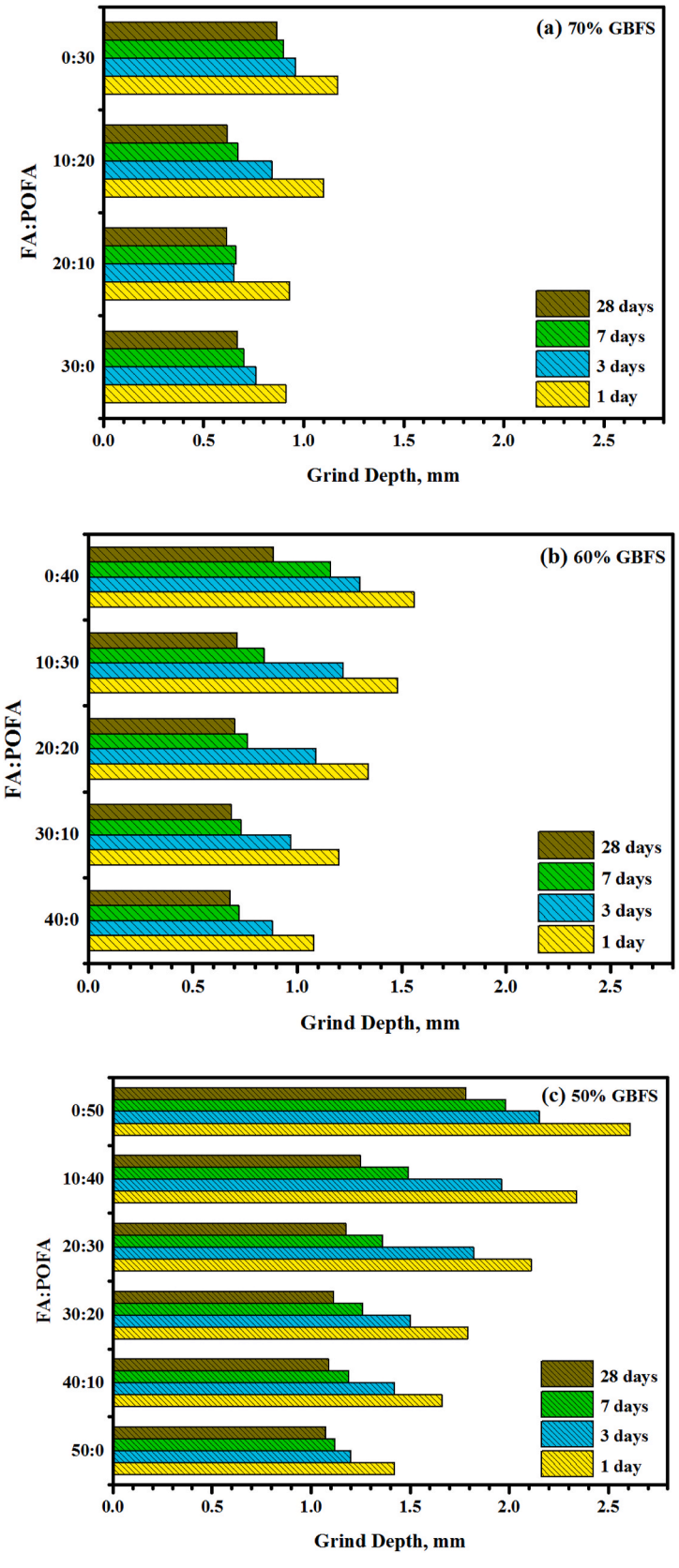

(caption on next page)

Fig. 26. High GBFS contents dependent measured grinding depths of AAMs (a) 70% GBFS (b) 60% GBFS (c) 50% GBFS.

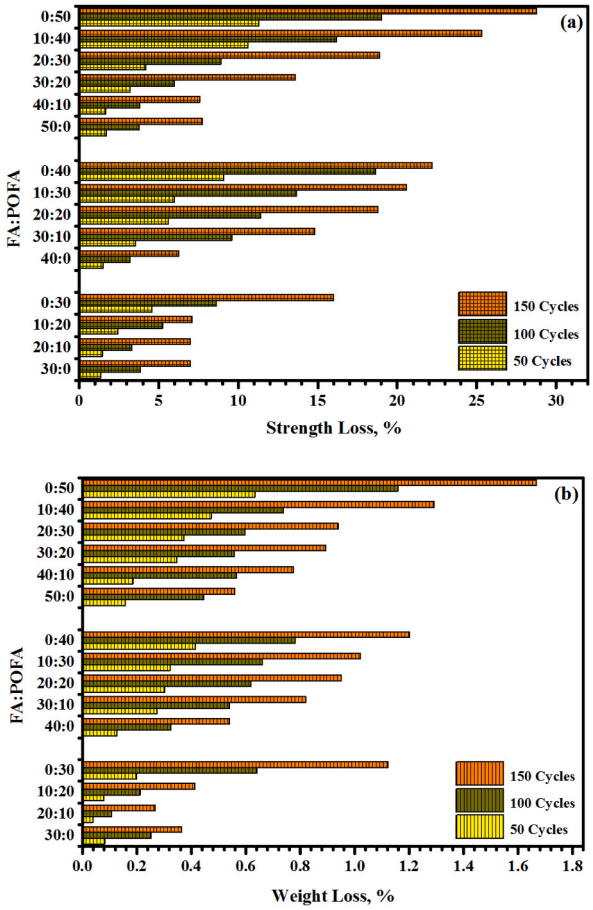

Fig. 27. Effect of high volume GBFS on the AAMs resistance against the deterioration under wet/dry cycles (a) strength loss (b) weight loss.

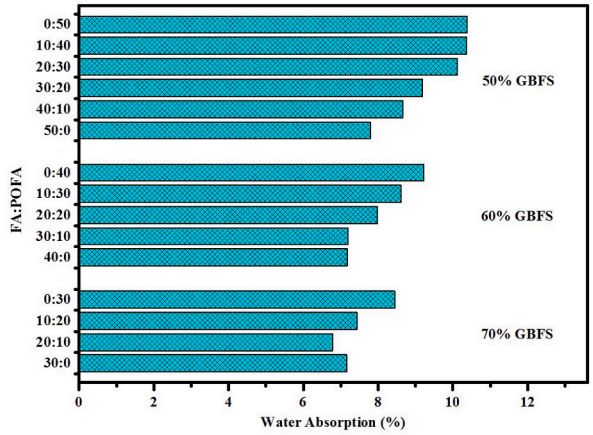

Fig. 28. High GBFS contents dependent WA of AAMs.

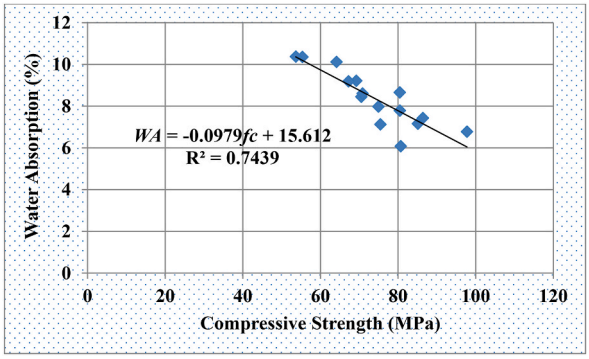

Fig. 29. Correlation of WA and CS of FA-POFA based AAMs incorporating high volume GBFS.

v. Inclusion of GBFS at high volume in the mortars could significantly improve the resistance against freeze/thaw and wet/dry cycles. This increase of GBFS in the mortars reduced the number of pores, enhancing its performance against aggressive environments. The specimens prepared with 70% of GBFS achieved the highest performance compared to other samples.
vi. It's found the abrasion resistance of alkali-activated specimens enhanced with raising GBFS content in ternary blended of alkali-activated from 50%, 60% and 70%.
vii. The increment in gels formulation with increasing GBFS led to improve the specimens' surface morphology and reduce the water abrasion percentage.
viii. The reduction in water abrasion capacity of the AAMs led to an improvement in their resistance against abrasion forces, freeze/thaw and wet-dry cycles.

Author contribution statement

Ghasan Fahim Huseien, Masoumeh khamehchi: Analyzed and interpreted the data; Wrote the paper.
Ziyad Kubba: Conceived and designed the experiments; Contributed reagents, materials, analysis tools or data.
Omrane Benjeddou: Conceived and designed the experiments; Performed the experiments.
Mohammad Javad Mahmoodi: Performed the experiments; Contributed reagents, materials, analysis tools or data.

Data availability statement

Data will be made available on request.

Declaration of competing interest

The authors declare that they have no known competing financial interests or personal relationships that could have appeared to influence the work reported in this paper

Acknowledgments

This study is supported via funding from Prince Sattam bin Abdulaziz University project number (PSAU/2023/R/1444).

References

[1] E. Khankhaje, M.W. Hussin, J. Mirza, M. Rafieizonooz, M.R. Salim, H.C. Siong, M.N.M. Warid, On blended cement and geopolymer concretes containing palm oil fuel ash, Mater. Des. 89 (2016) 385–398.
[2] A.M. Mhaya, S. Baharom, G.F. Huseien, Improved strength performance of rubberized Concrete: role of ground blast furnace slag and waste glass bottle nanoparticles amalgamation, Construct. Build. Mater. 342 (2022), 128073.
[3] W. Li, E.D. Shumuye, T. Shiying, Z. Wang, K. Zerfu, Eco-friendly fibre reinforced geopolymer concrete: a critical review on the microstructure and long-term durability properties, Case Stud. Constr. Mater. (2022), e00894.
[4] M.A. Asaad, G.F. Huseien, M.H. Baghban, P.B. Raja, R. Fediuk, I. Faridmehr, F. Alrshoudi, Gum Arabic nanoparticles as green corrosion inhibitor for reinforced concrete exposed to carbon dioxide environment, Materials 14 (2021) 7867.
[5] C. Ouellet-Plamondon, G. Habert, Life cycle assessment (LCA) of alkali-activated cements and concretes, in: Handbook of Alkali-Activated Cements, Mortars and Concretes, Elsevier, 2015, pp. 663–686.
[6] L.K. Turner, F.G. Collins, Carbon dioxide equivalent (CO2-e) emissions: a comparison between geopolymer and OPC cement concrete, Construct. Build. Mater. 43 (2013) 125–130.
[7] J.S. van Deventer, J.L. Provis, P. Duxson, D.G. Brice, Chemical research and climate change as drivers in the commercial adoption of alkali activated materials, Waste and Biomass Valoriz. 1 (2010) 145–155.
[8] P. Duxson, J.L. Provis, G.C. Lukey, J.S. Van Deventer, The role of inorganic polymer technology in the development of 'green concrete, Cement Concr. Res. 37 (2007) 1590–1597.
[9] J.L. Provis, Alkali-activated materials, Cement Concr. Res. 114 (2018) 40–48.

[10] J. Oluwafemi, O. Ofuyatan, A. Adedeji, D. Bankole, L. Justin, Reliability assessment of ground granulated blast furnace slag/cow bone ash-based geopolymer concrete, J. Build. Eng. 64 (2023), 105620.
[11] D. Adak, M. Sarkar, S. Mandal, Structural performance of nano-silica modified fly-ash based geopolymer concrete, Construct. Build. Mater. 135 (2017) 430–439.
[12] G. Ma, Y. Yan, M. Zhang, J. Sanjayan, Effect of steel slag on 3D concrete printing of geopolymer with quaternary binders, Ceram. Int. 48 (2022) 26233–26247.
[13] P. Chokkalingam, H. El-Hassan, A. El-Dieb, A. El-Mir, Development and characterization of ceramic waste powder-slag blended geopolymer concrete designed using Taguchi method, Construct. Build. Mater. 349 (2022), 128744.
[14] V.O. Ozcelik, C.E. White, Nanoscale charge-balancing mechanism in alkali-substituted calcium–silicate–hydrate gels, J. Phys. Chem. Lett. 7 (2016) 5266–5272.
[15] J.L. Provis, J.S.J. Van Deventer, Geopolymers: Structures, Processing, Properties and Industrial Applications, Elsevier, 2009.
[16] M. Morsy, S. Alsayed, Y. Al-Salloum, T. Almusallam, Effect of sodium silicate to sodium hydroxide ratios on strength and microstructure of fly ash geopolymer binder, Arabian J. Sci. Eng. 39 (2014) 4333–4339.
[17] J. Yang, H. Bai, X. He, J. Zeng, Y. Su, X. Wang, H. Zhao, C. Mao, Performances and microstructure of one-part fly ash geopolymer activated by calcium carbide slag and sodium metasilicate powder, Construct. Build. Mater. 367 (2023), 130303.
[18] M.T. Marvila, A.R.G. de Azevedo, L.B. de Oliveira, G. de Castro Xavier, C.M.F. Vieira, Mechanical, physical and durability properties of activated alkali cement based on blast furnace slag as a function of% Na2O, Case Stud. Constr. Mater. 15 (2021), e00723.
[19] M.T. Marvila, A.R.G. de Azevedo, J.A.L. Junior, C.M.F. Vieira, Activated alkali cement based on blast furnace slag: effect of curing type and concentration of Na20, J. Mater. Res. Technol. 23 (2023) 4551–4565.
[20] P. Zhang, Z. Gao, J. Wang, J. Guo, S. Hu, Y. Ling, Properties of fresh and hardened fly ash/slag based geopolymer concrete: a review, J. Clean. Prod. 270 (2020), 122389.
[21] W. Huang, H. Wang, Geopolymer pervious concrete modified with granulated blast furnace slag: microscale characterization and mechanical strength, J. Clean. Prod. 328 (2021), 129469.
[22] S. Singh, S.K. Sharma, M.A. Akbar, Developing zero carbon emission pavements with geopolymer concrete: a comprehensive review, Transport. Res. Transport Environ. 110 (2022), 103436.
[23] A. ASTM C618, Standard Specification for Coal Fly Ash and Raw or Calcined Natural Pozzolan for Use in Concrete, ASTM international, 2019.
[24] I. Ismail, S.A. Bernal, J.L. Provis, R. San Nicolas, S. Hamdan, J.S. van Deventer, Modification of phase evolution in alkali-activated blast furnace slag by the incorporation of fly ash, Cement Concr. Compos. 45 (2014) 125–135.
[25] ASTM, Standard Test Method for Materials Finer than 75-μm (No. 200) Sieve in Mineral Aggregates by Washing, ASTM C117-13, 2013.
[26] C. ASTM, Standard Specification for Concrete Aggregates, American Society for Testing and Materials, Philadelphia, PA, 2003.
[27] C. ASTM, Standard Test Method for Compressive Strength of Hydraulic Cement Mortars (Using 2-in. Or [50-mm] Cube Specimens), American Society for Testing and Material, 2002.
[28] A.S.f. Testing, Materials. Standard Test Method for Resistance of Concrete to Rapid Freezing and Thawing, 2015.
[29] A. Standard, Standard Test Method for Density, Absorption, and Voids in Hardened Concrete, ASTM Standard C, 2006, p. 642.
[30] C.K. Yip, G. Lukey, J. Van Deventer, The coexistence of geopolymeric gel and calcium silicate hydrate at the early stage of alkaline activation, Cement Concr. Res. 35 (2005) 1688–1697.
[31] A. Buchwald, H. Hilbig, C. Kaps, Alkali-activated metakaolin-slag blends—performance and structure in dependence of their composition, J. Mater. Sci. 42 (2007) 3024–3032.
[32] F. Pacheco-Torgal, J. Castro-Gomes, S. Jalali, Investigations on mix design of tungsten mine waste geopolymeric binder, Construct. Build. Mater. 22 (2008) 1939–1949.
[33] S. Kumar, R. Kumar, S. Mehrotra, Influence of granulated blast furnace slag on the reaction, structure and properties of fly ash based geopolymer, J. Mater. Sci. 45 (2010) 607–615.
[34] M.H. Al-Majidi, A. Lampropoulos, A. Cundy, S. Meikle, Development of geopolymer mortar under ambient temperature for in situ applications, Construct. Build. Mater. 120 (2016) 198–211.
[35] S. Kumar, R. Kumar, S. Mehrotra, Influence of granulated blast furnace slag on the reaction, structure and properties of fly ash based geopolymer, J. Mater. Sci. 45 (2010) 607–615.
[36] R. Yu, P. Spiesz, H. Brouwers, Development of an eco-friendly Ultra-High Performance Concrete (UHPC) with efficient cement and mineral admixtures uses, Cement Concr. Compos. 55 (2015) 383–394.
[37] S. Nath, S. Kumar, Influence of iron making slags on strength and microstructure of fly ash geopolymer, Construct. Build. Mater. 38 (2013) 924–930.
[38] M.B. Karakoç, I. Turkmen, M.M. Maraş, F. Kantarci, R. Demirboga, M.U. Toprak, Mechanical properties and setting time of ferrochrome slag based geopolymer paste and mortar, Construct. Build. Mater. 72 (2014) 283–292.
[39] I. Richardson, A. Brough, G. Groves, C. Dobson, The characterization of hardened alkali-activated blast-furnace slag pastes and the nature of the calcium silicate hydrate (CSH) phase, Cement Concr. Res. 24 (1994) 813–829.
[40] R.J. Myers, S.A. Bernal, R. San Nicolas, J.L. Provis, Generalized structural description of calcium–sodium aluminosilicate hydrate gels: the cross-linked substituted tobermorite model, Langmuir 29 (2013) 5294–5306.
[41] Z. Li, S. Liu, Influence of slag as additive on compressive strength of fly ash-based geopolymer, J. Mater. Civ. Eng. 19 (2007) 470–474.
[42] N. Ranjbar, M. Mehrali, A. Behnia, U.J. Alengaram, M.Z. Jumaat, Compressive strength and microstructural analysis of fly ash/palm oil fuel ash based geopolymer mortar, Mater. Des. 59 (2014) 532–539.
[43] M. Mijarsh, M.M. Johari, Z.A. Ahmad, Compressive strength of treated palm oil fuel ash based geopolymer mortar containing calcium hydroxide, aluminum hydroxide and silica fume as mineral additives, Cement Concr. Compos. 60 (2015) 65–81.
[44] G.F. Huseien, M.A. Asaad, A.A. Abadel, S.K. Ghoshal, H.K. Hamzah, O. Benjeddou, J. Mirza, Drying shrinkage, sulphuric acid and sulphate resistance of high-volume palm oil fuel ash-included alkali-activated mortars, Sustainability 14 (2022) 498.
[45] M. Ariffin, M. Azreen, M.W. Hussin, M.A. Rafique Bhutta, Mix design and compressive strength of geopolymer concrete containing blended ash from agro-industrial wastes, in: Proceedings of the Advanced Materials Research, 2011, pp. 452–457.
[46] S. Kabir, U.J. Alengaram, M.Z. Jumaat, A. Sharmin, A. Islam, Influence of molarity and chemical composition on the development of compressive strength in POFA based geopolymer mortar, Adv. Mater. Sci. Eng. 2015 (2015).
[47] A. Islam, U.J. Alengaram, M.Z. Jumaat, I.I. Bashar, S.A. Kabir, Engineering properties and carbon footprint of ground granulated blast-furnace slag-palm oil fuel ash-based structural geopolymer concrete, Construct. Build. Mater. 101 (2015) 503–521.
[48] P. Chindaprasirt, P. De Silva, K. Sagoe-Crentsil, S. Hanjitsuwan, Effect of SiO2 and Al2O3 on the setting and hardening of high calcium fly ash-based geopolymer systems, J. Mater. Sci. 47 (2012) 4876–4883.
[49] A. Fernandez-Jimenez, A. Palomo, Mid-infrared spectroscopic studies of alkali-activated fly ash structure, Microporous Mesoporous Mater. 86 (2005) 207–214.
[50] J. Marchand, M. Pigeon, D. Bager, C. Talbot, Influence of chloride solution concentration on deicer salt scaling deterioration of concrete, Materials Journal 96 (1999) 429–435.
[51] Z. Liu, W. Hansen, Freezing characteristics of air-entrained concrete in the presence of deicing salt, Cement Concr. Res. 74 (2015) 10–18.
[52] R. Mohebi, K. Behfarnia, M. Shojaei, Abrasion resistance of alkali-activated slag concrete designed by Taguchi method, Construct. Build. Mater. 98 (2015) 792–798.